Chemistry Europe
European Chemical Societies Publishing

WILEY VCH

Excellence in Chemistry Research

Announcing our new flagship journal

- Gold Open Access
- Publishing charges waived
- Preprints welcome
- Edited by active scientists

Meet the Editors of *ChemistryEurope*

Luisa De Cola
Università degli Studi di Milano Statale, Italy

Ive Hermans
University of Wisconsin-Madison, USA

Ken Tanaka
Tokyo Institute of Technology, Japan

ChemCatChem

Research Article
doi.org/10.1002/cctc.202300055

Chemistry Europe
European Chemical Societies Publishing

www.chemcatchem.org

Computational Discovery of Active and Selective Metal-Nitrogen-Graphene Catalysts for Electrooxidation of Water to H_2O_2

Payal Chaudhary,[a] Iman Evazzade,[a] Rodion Belosludov,[b, c] and Vitaly Alexandrov*[a, d]

A direct electrosynthesis of H_2O_2 from either O_2 or H_2O is an attractive strategy to replace the energy-intensive industrial anthraquinone process. Two-electron water oxidation reaction (2e-WOR) offers several advantages over the oxygen reduction reaction such as better mass transfer due to the absence of gas-phase reactants. However, 2e-WOR is a more challenging and less studied process with only a handful of metal oxides exhibiting reasonable activity/selectivity properties. Herein, we employ density-functional-theory calculations to screen a variety of metal-nitrogen-graphene structures for 2e-WOR. As a consequence of scaling between the adsorption energies of reaction intermediates, we determine a linear relation between selectivities for the first and second reaction steps of 2e-WOR, viz. that if selectivity toward adsorbed OH is improved, then selectivity toward H_2O_2 at the subsequent step is decreased. We also find that selectivity and activity are linearly scaled in such a way that a higher activity (i.e., a lower overpotential) leads to a lower selectivity for the H_2O_2 formation step. Based on the obtained results several chemistries, e.g., containing NiN_x–C moieties, are predicted to rival the best-performing metal oxides such as ZnO and $CaSnO_3$ in terms of combination of their activity/selectivity characteristics for 2e-WOR.

Introduction

Hydrogen peroxide (H_2O_2) is one of the most valuable chemicals in modern chemical industry. At present, it is synthesized using the energy-intensive process based on sequential reduction and oxidation of an alkylated anthraquinone.[1] Electrochemical production of H_2O_2 presents a sustainable and cost-effective alternative route.[2–4] There are two main electrochemical ways to produce H_2O_2 starting either from O_2 (two-electron oxygen reduction reaction, 2e-ORR):

$$O_2 + 2(H^+ + e^-) \rightarrow H_2O_2 \qquad E^0 = 1.76\ V_{RHE} \tag{1}$$

or from H_2O (two-electron water oxidation reaction, 2e-WOR):

$$2H_2O + H_2O_2 + 2(H^+ + e^-) \qquad E^0 = 1.70\ V_{RHE} \tag{2}$$

The first approach (2e-ORR) has gained a lot of scientific attention in the past.[2–11] The second approach (2e-WOR) is an appealing alternative as the process can be combined with the hydrogen evolution reaction (HER) to simultaneously produce two valuable products, H_2O_2 and H_2, in a single electrochemical system using only H_2O as a starting material. As a homogeneous reaction with no gas-phase reactants 2e-WOR offers other advantages over 2e-ORR such as better mass transfer. Until now, 2e-WOR has received by far less attention than 2e-ORR with only a few metal oxides analyzed in detail.[2–4, 12–14]

One key problem for efficient electrochemical production of H_2O_2 is the reaction selectivity. For example, in the case of WOR three reactions can occur, namely, the one-electron pathway leading to aqueous OH:

$$* + H_2O \rightarrow {}^*OH + (H^+ + e^-) \tag{3a}$$

$${}^*OH \rightarrow OH_{aq} \tag{3b}$$

the two-electron pathway resulting in H_2O_2:

$$* + H_2O \rightarrow {}^*OH + (H^+ + e^-) \tag{4a}$$

$${}^*OH + H_2O \rightarrow H_2O_2 + (H^+ + e^-) \tag{4b}$$

and the four-electron pathway of O_2 generation:

[a] P. Chaudhary, Dr. I. Evazzade, Prof. Dr. V. Alexandrov
Department of Chemical and Biomolecular Engineering
University of Nebraska-Lincoln
Lincoln, Nebraska 68588, United States
E-mail: valexandrov2@unl.edu
[b] Prof. Dr. R. Belosludov
Department of Materials Science and Engineering
Tohoku University
Sendai, Japan
[c] Prof. Dr. R. Belosludov
Institute for Materials Research
Tohoku University
Sendai, Japan
[d] Prof. Dr. V. Alexandrov
Nebraska Center for Materials and Nanoscience
University of Nebraska-Lincoln
Lincoln, Nebraska 68588, United States
E-mail: valexandrov2@unl.edu

Supporting information for this article is available on the WWW under https://doi.org/10.1002/cctc.202300055

$$^{*} + H_2O \rightarrow {}^{*}OH + (H^{+} + e^{-}) \quad (5a)$$

$$^{*}OH \rightarrow {}^{*}O + (H^{+} + e^{-}) \quad (5b)$$

$$^{*}O + H_2O \rightarrow {}^{*}OOH + (H^{+} + e^{-}) \quad (5c)$$

$$^{*}OOH \rightarrow {}^{*} + O_2 + (H^{+} + e^{-}) \quad (5d)$$

Moreover, there could be other deleterious reactions such as the spontaneous disproportionation of H_2O_2 to H_2O and O_2 reducing the overall H_2O_2 yield. Also, the role of electrolyte species such as bicarbonate HCO_3^- in the catalytic mechanism of H_2O_2 formation remains poorly understood.[12] Nevertheless, a significant advantage of H_2O_2 synthesis over other approaches is that the reaction side products are simply H_2O and O_2 making it a great avenue for research.

Recent density-functional-theory (DFT) based investigations have focused on identifying good candidates for H_2O_2 production via materials screening by constructing free energy diagrams within the computational hydrogen electrode (CHE) approach.[3,6,13–17] These computational studies combined with experiments revealed that it is indeed possible to achieve high selectivity for electrochemical production of H_2O_2 via both 2e-ORR and 2e-WOR.

In the case of cathodic 2e-ORR over metal alloys, it was demonstrated that some compounds such as $PtHg_4$ intermetallic can be both active and selective towards H_2O_2 production.[6,8] This was attributed to the so-called ensemble effect that turned out to be an efficient way to control H_2O_2 selectivity. Specifically, it was shown that four inactive Hg atoms surrounding the surface Pt atom break the Pt–Pt–Pt active motifs leading to a substantial weakening of O adsorption. This occurs by making the top Pt surface site in $PtHg_4$ more favorable for O adsorption than the face-centered-cubic (fcc) hollow site of the pure Pt metal. Subsequent high-throughput DFT based calculations led to the discovery of other promising metal alloys for highly selective H_2O_2 formation via 2e-ORR.[17] Unfortunately, most alloys identified so far contain expensive (e.g., Pt, Au and Pd) or eco-unfriendly (e.g., Hg) species.

In the case of anodic H_2O_2 synthesis via 2e-WOR, there is only a limited number of metal oxides selective toward H_2O_2 with several systems approaching the theoretical maximum such as WO_3, ZnO, and $CaSnO_3$.[3,18] A series of previous DFT based theoretical studies focusing on metal oxides provided important insights into the issue of H_2O_2 selectivity. Thermodynamically, in terms of OH and O binding energies the systems with favorable selectivity towards H_2O_2 evolution via 2e-WOR should satisfy the following two criteria: $\Delta G^{*}_{O} \geq 3.52$ eV and $1.76\ \text{eV} \leq \Delta G^{*}_{OH} \leq 2.4$ eV. However, due to the linear scaling relationship between ΔG^{*}_{O} and ΔG^{*}_{OH} a real region for selective H_2O_2 formation becomes much smaller than the one defined by the two thermodynamics criteria. These thermodynamic considerations significantly limit the number of metal oxides that can be H_2O_2 selective via 2e-WOR.

This motivates our present DFT study aimed at identifying Pt-group metal free (PGM-free) catalysts based on N-doped graphene for active and selective electrochemical synthesis of H_2O_2 through water oxidation. In recent years, carbon-based catalysts including graphene-based single-atom catalysts (SACs) have gained significant attention.[19,20] Not only was their catalytic activity toward a variety of reactions examined, but also their electrochemical stability under both acidic and alkaline conditions.[21–25] In this work, we consider a diverse set of basal- and edge-surface structures with single- (MN_x–C) and dual-metal ($M_1M_2N_x$–C) active centers embedded into the graphene matrix. By analyzing both mono- and bi-nuclear mechanisms of H_2O_2 formation via 2e-WOR we reveal a number of highly active and selective chemistries such as those based on the NiN_x–C frameworks. We note that unlike SACs, dual-metal centers in the N-doped graphene are much less investigated, but it was demonstrated that such catalysts can be synthesized and provide superior catalytic activity than SACs. For example, the graphene-based dual-metal $FeCoN_5$-OH catalyst was shown to deliver an intrinsic activity toward ORR over 20 times higher than single-atom FeN_4.[26]

Results and Discussion

We start by analyzing the mono-nuclear mechanism of water oxidation schematically shown in Figure 1. The figure displays the one-, two- and four-electron reaction steps, i.e., involving *OH, *O, and *OOH intermediates, as described by Eqs. (3–5). The corresponding DFT derived free energy diagrams for several representative single-metal catalysts are provided in Figure 2. Following the established computational approach,[3,18] the energies of the final state, i.e., solvated OH ($\Delta G_{OH_{aq}} = 2.4$ eV), solvated H_2O_2 ($\Delta G_{H_2O_2} = 3.52$ eV) and gas-phase O_2 ($\Delta G_{O_2} = 4.92$ eV) for these diagrams are taken from experiments. Figure 2 demonstrates the point that the reaction pathway strongly depends on the nature of the transition-metal center even for the same atomic configuration MN_x–C (4) (see the atomic structure in Figure 9). It can be seen for the first reaction step that the formation of adsorbed OH is more favorable than

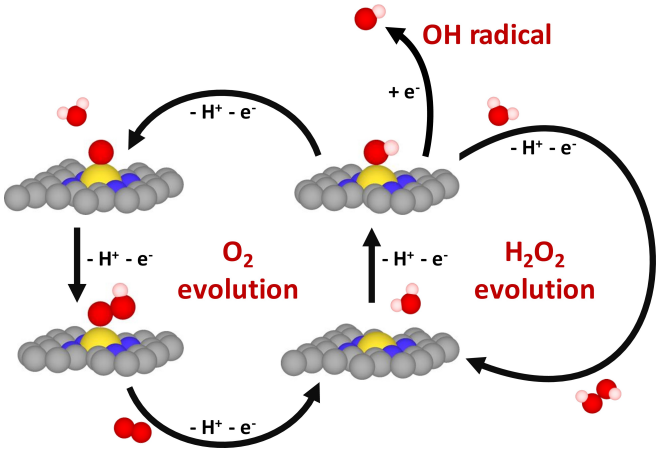

Figure 1. Schematic showing the competing reactions of water oxidation via 1-, 2- and 4-electron pathways that lead to the formation of OH, H_2O_2 and O_2 products, respectively.

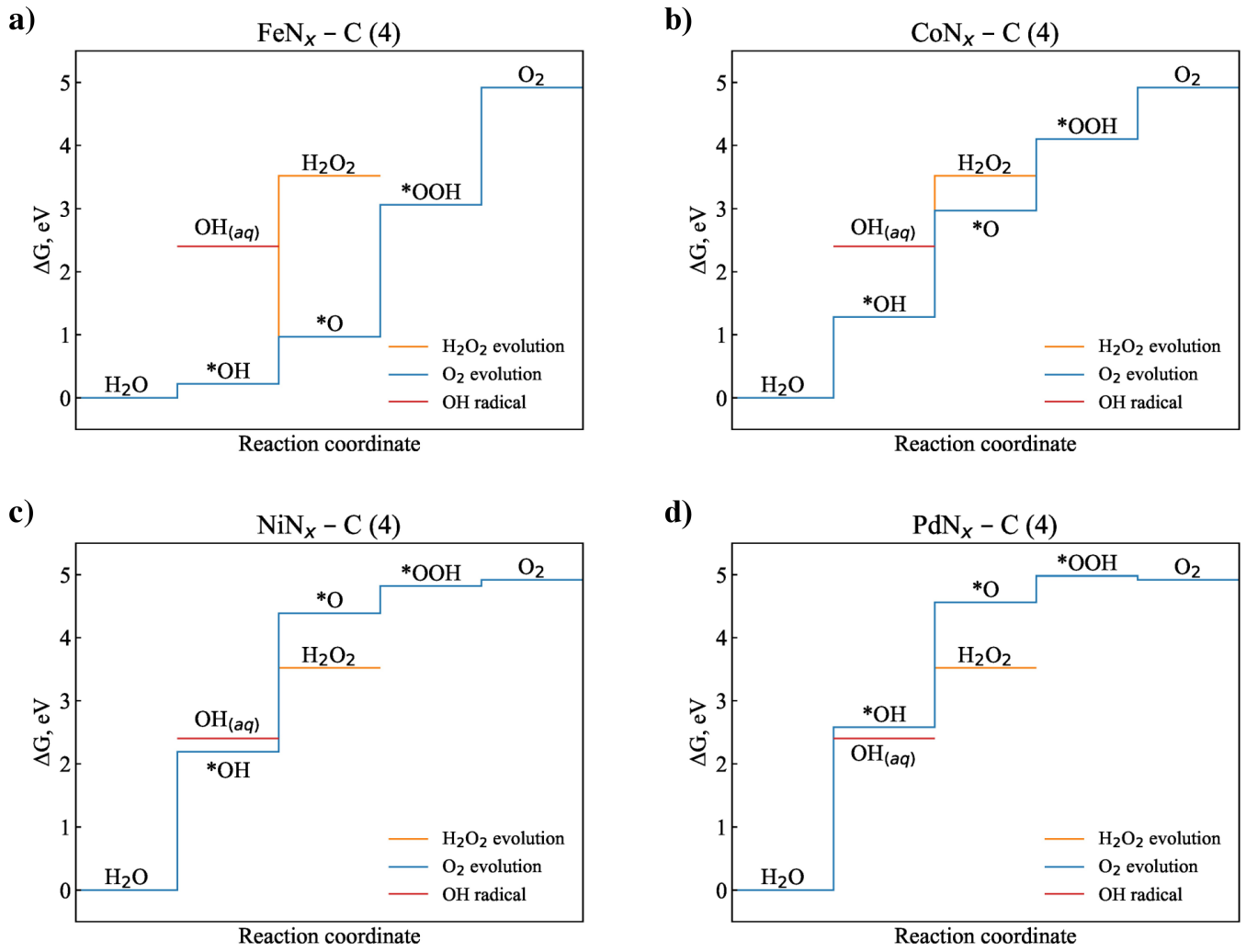

Figure 2. Free energy diagrams for 1e-, 2e-, and 4e-WOR pathways on the example of structure (4) for FeN_x- (a), CoN_x- (b), NiN_x- (c) and PdN_x-doped (d) graphene catalysts (see Figure 9).

that of aqueous OH for the Fe-, Co- and Ni-based systems, while the opposite is true for Pd. For the second step, the formation of adsorbed O is preferred over H_2O_2 for the Fe- and Co-based catalysts promoting the complete four-electron oxidation to O_2, whereas the Ni and Pd systems have a higher propensity for H_2O_2 evolution.

Within this free energy diagram formalism, the difference between theoretical overpotentials estimated for different reaction pathways can serve as a measure of reaction selectivity. Specifically, following previous computational studies,[3,18] we can define:

$$\Delta\eta(^{*}\mathrm{OH}) = (\Delta G_{\mathrm{OH_{aq}}} - \Delta G{*}_{\mathrm{OH}})/e = (2.4 - \Delta G{*}_{\mathrm{OH}})/e \quad (6)$$

as a selectivity metric for *OH formation during the first reaction step, and:

$$\Delta\eta(\mathrm{H_2O_2}) = (\Delta G{*}_{\mathrm{O}} - \Delta G_{\mathrm{H_2O_2}})/e = (\Delta G{*}_{\mathrm{O}} - 3.52)/e \quad (7)$$

as a selectivity metric for H_2O_2 formation during the second step. For example, a prior DFT study found that the formation of H_2O_2 is by far more favorable than the formation of *O over the TiO_2(110) surface.[18] On the other hand, it was calculated that the formation of adsorbed OH and desorption of OH radical should be almost equiprobable. Therefore, the first reaction step would limit the overall H_2O_2 selectivity in the case of TiO_2(110). These computational results appear to agree with some experimental reports showing the formation of OH radicals together with a small amount of H_2O_2 for UV illuminated TiO_2.[27,28] Ideally, both $\Delta\eta$(*OH) and $\Delta\eta(H_2O_2)$ should be maximized for optimal H_2O_2 production. However, it turns out to be challenging to independently increase $\Delta\eta$(*OH) and $\Delta\eta(H_2O_2)$ due to linear scaling relationships between the binding energies of reaction intermediates as discussed below.

Figure 3 shows two-dimensional selectivity maps for the mono-nuclear mechanism of WOR over single- (MN_x–C) and dual-metal ($M_1M_2N_x$–C) catalysts as derived from our DFT simulations. Constructed in terms of the binding energies of the *O and *OH reaction intermediates, the maps depict three

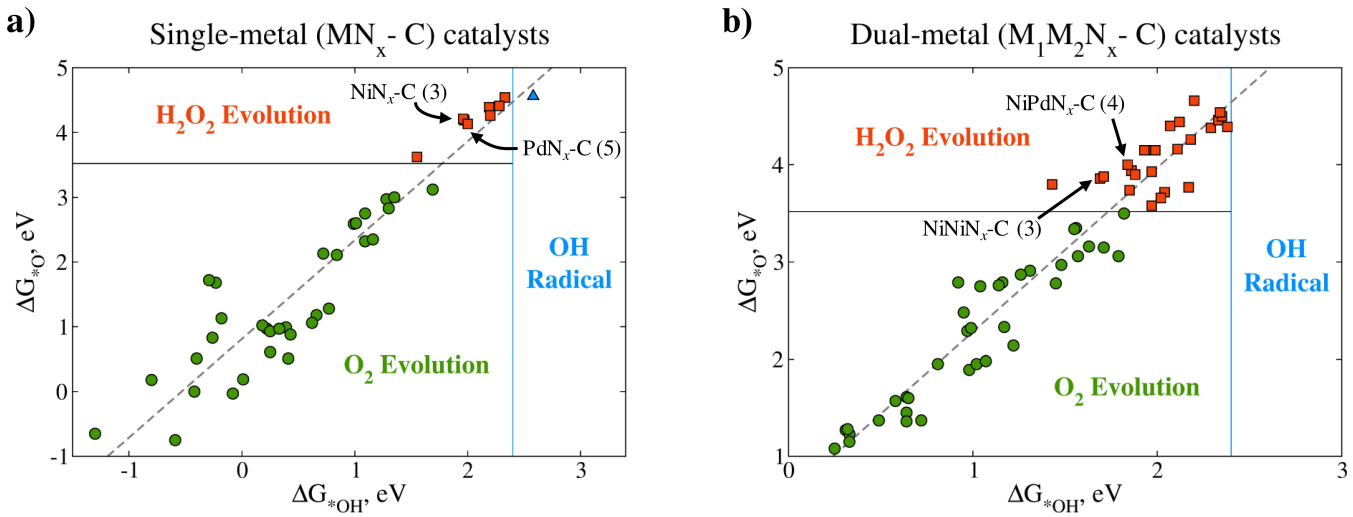

Figure 3. Two-dimensional product selectivity maps for both single- (a) and dual-metal (b) systems in terms of the adsorption energies of *O vs. *OH. The maps show regions with preferential formation of OH, H_2O_2 or O_2 based on reaction thermodynamics limitations. The dashed lines depict the scaling line between $\triangle G$(*O) and $\triangle G$(*OH).

regions of selectivity corresponding to thermodynamically favorable production of OH, H_2O_2 and O_2. Due to the known linear scaling relationship between $\Delta G*_O$ and $\Delta G*_{OH}$ a real region for selective H_2O_2 formation shrinks to a small corner. It is interesting to note that the slopes of the scaling line for the single- and dual-metal catalysts in this work are estimated at 1.5 and 1.6, respectively, being comparable to the slope of 1.5 found previously for metal-oxide catalysts.[3] Despite all these thermodynamic limitations, our results reveal quite a multitude of doped-graphene chemistries that fall into the H_2O_2 selectivity domain.

As pointed out above, ideally, to maximize the yield of H_2O_2 via 2e-WOR, selectivity to both the first reaction step to produce *OH and the second step to form H_2O_2 should be as high as possible. Our results, however, demonstrate, that this is challenging to achieve due to the linear correlation between $\Delta\eta$(*OH) and $\Delta\eta(H_2O_2)$ as shown in Figure 4. These plots illustrate that it is impossible to independently enhance $\Delta\eta$(*OH) and $\Delta\eta(H_2O_2)$ for both single- and dual-metal catalysts considered in this study. Namely, if selectivity toward *OH is improved, i.e., $\Delta\eta$(*OH) is increased, then selectivity toward H_2O_2 is compromised as $\Delta\eta(H_2O_2)$ becomes decreased. This result is a direct consequence of the scaling relationship between $\Delta G*_O$ and $\Delta G*_{OH}$ as can be clearly seen from Eqs. (6) und (7). Similarly, we can analyze the relationship between selectivity and activity for the second step of H_2O_2 formation (Figure 5). As expected from the scaling relations, we can see in

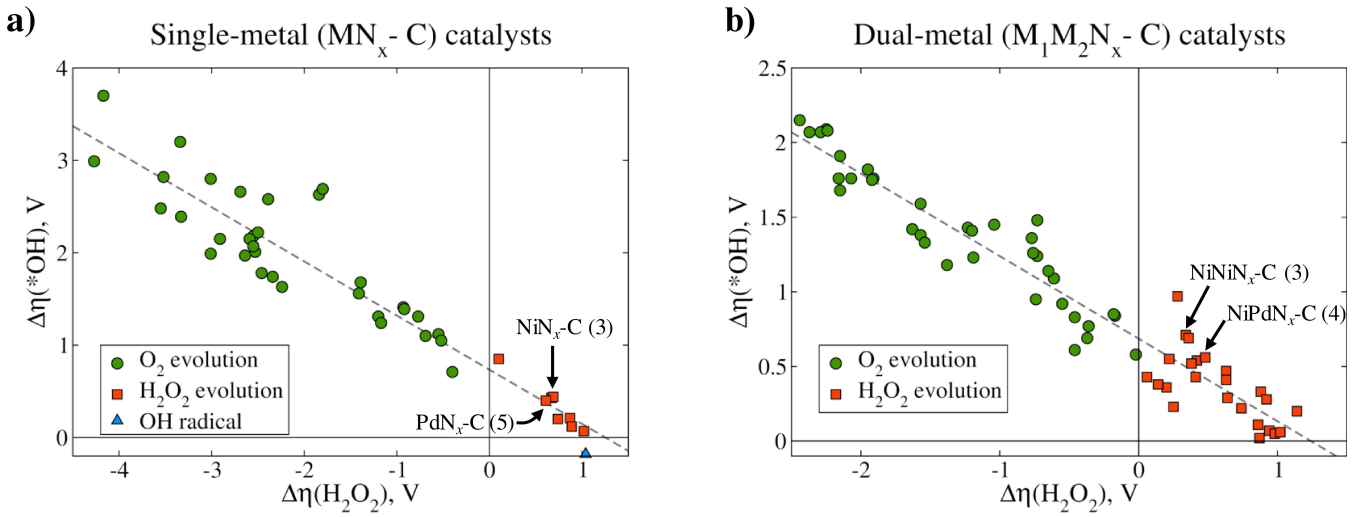

Figure 4. Linear scaling relations between selectivities for the first electron step yielding *OH and for the second electron step yielding H_2O_2 for the single- (a) and dual-metal (b) systems.

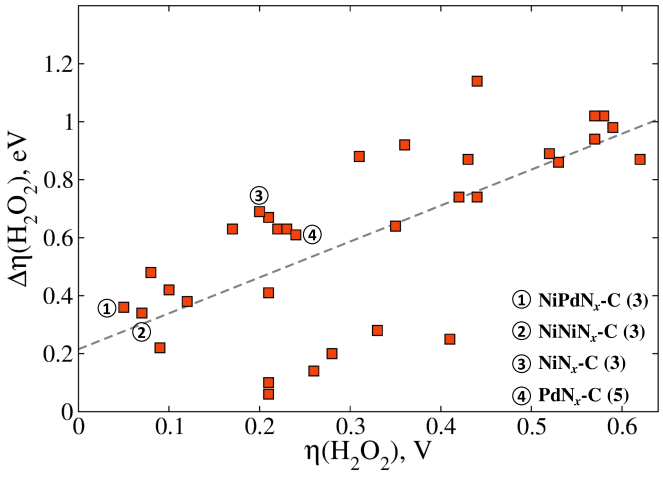

Figure 5. Linear scaling relation between selectivity ($\triangle\eta(H_2O_2)$) and activity (measured as theoretical overpotential $\eta(H_2O_2)$) for the H_2O_2 formation step. Several single- and dual-metal systems are highlighted.

the figure that when the reaction selectivity is increased, the reaction activity is decreased.

Out of all the data we have obtained for single- and dual-metal centers, we now pick a subset of the most promising structures in terms of their combination of activity and selectivity properties which we define here as $\eta \leq 0.3$ V and $\Delta\eta \geq 0.3$ V. This allows us to compare the best graphene-based catalysts identified in the present study with the state-of-the-art metal-oxide catalysts toward selective H_2O_2 production. Figure 6 shows the volcano plots depicting the computed limiting potential (U_L) for 2e- and 4e-WOR as a function of *OH binding energy ($\Delta G*_{OH}$). Here, following some previous theoretical studies,[3] U_L serves as a measure of H_2O_2 catalytic activity and is

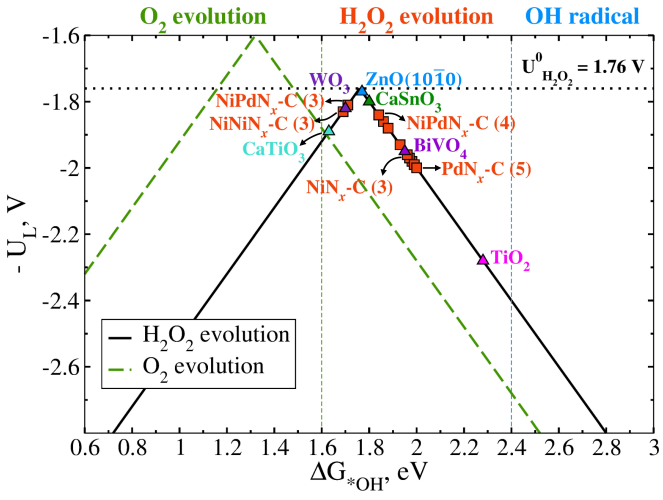

Figure 6. Volcano plots for the 2e-WOR (solid line) and 4e-WOR (dashed line) pathways showing activity trends for the best H_2O_2 selective systems identified in this study and some metal oxides from prior investigations. The corresponding equilibrium potential for 2e-WOR $U^0_{H_2O_2} = 1.76$ V_{RHE} and for 4e-WOR $U^0_{O_2} = 1.6$ V_{RHE}. Only the best graphene-based systems (with over-potentials lower than 0.3 V) identified in this study are shown.

defined as the lowest potential at which all the reaction elementary steps become thermoneutral. Thus, the reaction overpotential can be computed as $|U^0_{H_2O_2} - U_L|$, where $U^0_{H_2O_2}$ is the equilibrium potential for the 2e-WOR being 1.76 V_{RHE}. Table 1 presents the computed values for selectivity metrics for the first and second steps of the 2e-WOR and the overpotentials of the best performing graphene-based systems compared to the metal oxides found in previous studies. It can be clearly seen that some MN_x-doped graphene systems are predicted to elicit catalytic activities and reaction selectivities comparable to the best-performing ZnO(10$\bar{1}$0), WO_3 and $CaSnO_3$ catalysts.

It is well known that a specific choice of the exchange-correlation functional can affect the adsorption energies of reaction intermediates. This issue was also discussed in the case of graphene-based single-atom catalysts (SACs).[31,32] To check the sensitivity of our results, we additionally run calculations for our best catalysts using the rotationally invariant version of the PBE+U approach.[33] The Hubbard U parameters for graphene-based SACs were taken from Ref.[31] The obtained values are listed in Table 1 in parentheses for comparison. It can be clearly seen that the results do not change significantly thus supporting our main conclusions about activity-selectivity properties of doped-graphene catalysts examined in this work.

Having analyzed the mono-nuclear mechanism of H_2O_2 formation, we next consider the alternative bi-nuclear mechanism. Both reaction mechanisms are schematically shown in Figure 7. The bi-nuclear pathway may become feasible at dual-metal active centers when adsorbed *OH species at the neighboring sites are close enough to be able to recombine. We find, however, that the mono-nuclear mechanism is preferred for all the systems analyzed in this work with dissimilar metal centers. Nevertheless, the formation of H_2O_2 following the bi-nuclear mechanism becomes more favorable over catalysts with the same metal sites such as NiNiN$_x$–C. Figure 8 illustrates this point on the example of NiNiN$_x$–C (5).

Finally, we want to discuss a few important aspects of 2e-WOR. First, we stress that all our predictions are solely based on thermodynamic arguments similar to the majority of previous theoretical studies on reaction selectivity. It should be pointed out, however, that the reaction kinetics of H_2O_2 formation was found to play a key role in defining reaction selectivity in the case of ORR over some M–N–C catalysts. In particular, the basal-

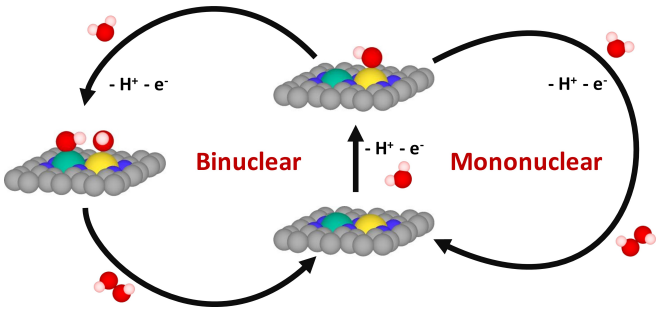

Figure 7. Schematic showing the competing reactions of water oxidation via 1-, 2- and 4-electron pathways that lead to the formation of OH, H_2O_2 and O_2 products, respectively.

Table 1. Activity and selectivity values for several best catalysts identified in the present study and comparison with some metal-oxide systems from published literature. The values obtained using the PBE+*U* approach with the Hubbard *U* parameters taken from Ref. [31] are provided in parentheses for comparison.

Structure	$\Delta\eta$(OH*), V	$\Delta\eta(H_2O_2)$, V	$\eta(H_2O_2)$, V
ZnO($10\bar{1}0$) (Ref. [29])	0.63	0.46	0.01
$CaSnO_3$ (Ref. [13])	0.60	–	0.04
WO_3 (Ref. [30])	0.70	0.30	0.06
$CaTiO_3$ (Ref. [30])	0.77	0.46	0.13
$BiVO_4$ (Ref. [18])	0.45	0.85	0.19
$SrTiO_3$ (Ref. [30])	0.83	0.40	0.19
TiO_2 (Ref. [18])	0.12	1.35	0.52
NiN_x–C (1)	0.43 (0.39)	0.67 (0.87)	0.21 (0.25)
NiN_x–C (3)	0.44 (0.44)	0.69 (0.69)	0.20 (0.20)
PdN_x–C (5)	0.40 (0.40)	0.61 (0.61)	0.24 (0.24)
$NiNiN_x$–C (3)	0.71 (0.71)	0.34 (0.41)	0.07 (0.07)
$NiPdN_x$–C (3)	0.69 (0.69)	0.36 (0.42)	0.05 (0.05)
$NiPdN_x$–C (4)	0.56 (0.48)	0.48 (0.57)	0.08 (0.16)

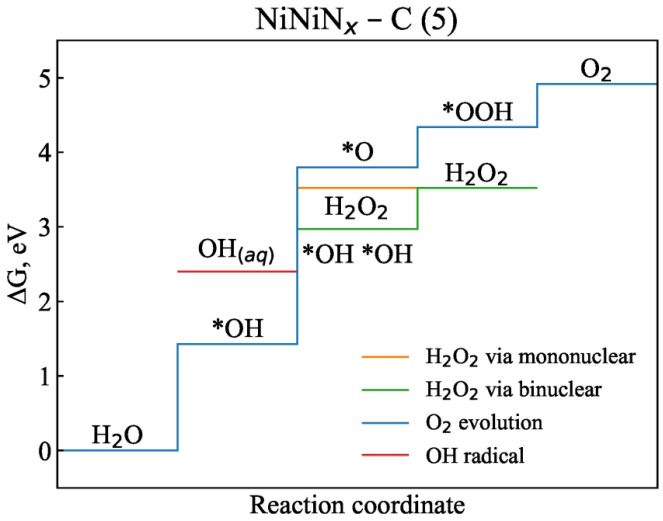

Figure 8. Free energy diagram for 1e-, 2e-, and 4e-WOR pathways comparing mono- and bi-nuclear reaction mechanisms of H_2O_2 formation for the $NiNiN_x$–C (5) system.

surface Co–N–C graphene catalyst gave rise to the experimental H_2O_2 selectivity ranging from 60% to 90%.[10] However, DFT simulations showed that breaking of the O–OH bond is thermodynamically more favorable than breaking of *–O by about 0.5 eV thus suggesting a low H_2O_2 selectivity.[34] A similar discrepancy was found for the Pd–Au alloy for which the selectivity towards H_2O_2 via ORR was measured as high as 95%, while DFT again predicted breaking of the O–OH bond by 0.3 eV easier than that of *–O.[35] To resolve this contraction with experimental observations, the constant-potential AIMD simulations of activation barriers for the corresponding bond-breaking events were undertaken in the case of the Co–N–C graphene-based catalyst.[16] The obtained results turned out to agree with experiments suggesting the kinetic origin of the observed H_2O_2 selectivity. Therefore, we believe that future computational studies should also analyze reaction kinetics for 2e-WOR catalysts. However, it might be expected that the systems characterized by large differences in thermodynamic overpotentials for both the *OH and H_2O_2 formation steps should remain as promising candidates for highly selective H_2O_2 production via 2e-WOR.

We also wish to comment on synthesis of transitional metal-nitrogen-carbon catalysts. The most common synthetic method is based on high temperature treatment (pyrolysis) of metal, nitrogen and carbon precursors in an inert atmosphere.[20] The principal problem of this approach is the formation of a multi-component mixture of carbonaceous products including a multitude of M–N–C moieties incorporated in the carbon matrix. In addition, the underlying mechanistic details of the process are still not well understood making it more of a "black-box" method and thus limiting the level of control over the pyrolysis products. Our present theoretical results reveal that activity and selectivity properties depend strongly on M–N–C chemistry and structure. Alternative synthetic approaches can enable a higher level of product control to maximize the content of best-performing M–N–C moieties in the graphene matrix. Recent experimental advances hold a lot of promise in terms of controllable synthesis and accurate characterization of such catalytic systems.[36–38]

Conclusion

In this work, we employed DFT simulations to examine a pool of single- and dual-metal N-doped graphene structures as candidates for selective electrosynthesis of H_2O_2 via 2-electron water oxidation reaction (2e-WOR). Our thermodynamic analysis of the competing reactions (1-, 2- and 4-electron processes) enabled identification of a series of promising catalysts, in particular, those based on NiN_x moieties within the graphene structure. Some systems are predicted to rival the best-performing metal oxides such as ZnO and $CaSnO_3$ in terms of combination of their activity/selectivity properties for 2e-WOR. We note that our screening is by far not exhaustive leaving a lot of space for further exploration of carbon-based materials. Nevertheless, the study does demonstrate the ability of M–N–C systems to efficiently catalyze water oxidation to produce H_2O_2.

Our findings also include the observation of two linear scaling relations as a direct consequence of scaling between

the adsorption energies of reaction intermediates. The first scaling relationship is between selectivities for the first reaction step yielding adsorbed *OH and the second step yielding H_2O_2. Specifically, it is found that if selectivity towards *OH is improved, then selectivity towards H_2O_2 is compromised. The second linear relationship is determined between activity and selectivity of H_2O_2 formation (the second reaction step) which is if activity is to be improved (i.e., by lowering overpotential), then selectivity is decreased. Therefore, in order to maximize selectivities during both reaction steps along with minimizing the reaction overpotentials, strategies for breaking these relationships should be sought out.

Further experimental studies are warranted to validate our catalyst predictions under real electrochemical conditions. We also point out that electrochemical stability and cost of catalysts are other key metrics that should be included in a more comprehensive analysis of electrocatalytic performance.

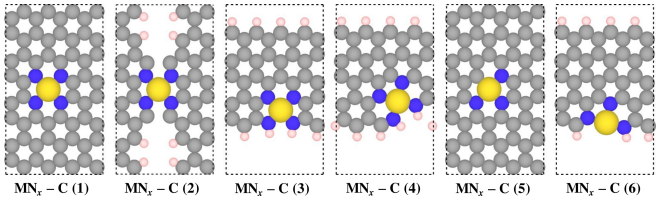

Figure 9. Top view of unit cells with single-metal nitrogen (MN_x–C) active centers embedded into the graphene matrix. The corresponding cell dimensions are listed in Table 2.

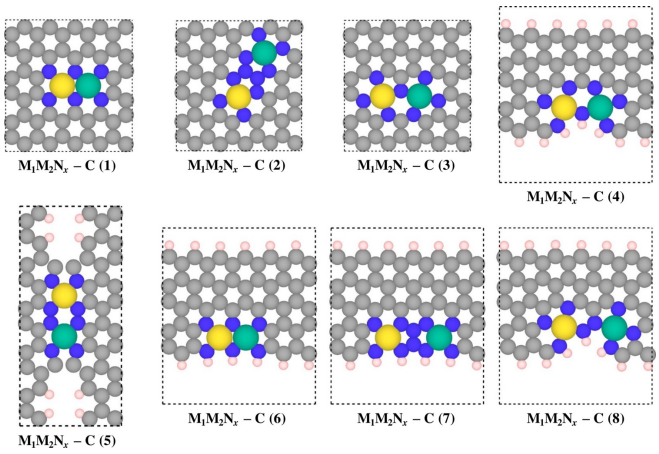

Figure 10. Top view of unit cells with dual-metal nitrogen ($M_1M_2N_x$–C) active centers embedded into the graphene matrix. The corresponding cell dimensions are listed in Table 2.

Table 2. Cell dimensions for single- and dual-metal N-doped graphene structures adopted in the present study (see Figures 9 and 10).

Label	Unit cell dimensions
MN_x–C (1-6)	a = 9.675 Å, b = 16.759 Å, c = 15.000 Å
$M_1M_2N_x$–C (1–3)	a = 12.259 Å, b = 12.740 Å, c = 15.000 Å
$M_1M_2N_x$–C (4)	a = 14.625 Å, b = 16.888 Å, c = 15.000 Å
$M_1M_2N_x$–C (5)	a = 9.807 Å, b = 21.233 Å, c = 15.000 Å
$M_1M_2N_x$–C (6–8)	a = 14.625 Å, b = 16.888 Å, c = 15.000 Å

Computational Approach

Figures 9 and 10 show unit cells for single- (MN_x–C) and dual-metal ($M_1M_2N_x$–C) active centers, respectively, embedded into the graphene matrix that are used in our simulations. The corresponding cell dimensions are provided in Table 2. To probe activity/selectivity properties of H_2O_2 formation via 2e-WOR, we chose a relatively rich pool of candidates comprised of a variety of basal- and edge-surface atomic structures that include 3*d* (M = Mn, Fe, Co and Ni) and 4*d* (M = Ru, Rh and Pd) transition metals. In total, we generated 42 single- (MN_x–C) and 61 dual-metal ($M_1M_2N_x$–C) configurations to examine.

All density-functional-theory (DFT) calculations were performed with the VASP code.[39,40] Spin-polarised calculations were carried out using the projector augmented wave (PAW) potentials[41] combined with the generalized gradient approximation (GGA) as formulated in the Perdew–Burke–Ernzerhof (PBE) exchange-correlation functional.[42,43] Corrections for non-local van der Waals interactions were applied using the Grimme's DFT-D3 approximation.[44] A plane-wave cutoff energy of 400 eV and Fermi smearing with a smearing width of 0.2 eV were employed. The k-point mesh for each structure was generated using the VASPKIT code[45] with the Γ-centered k-mesh scheme and a k-mesh-resolved value of $2\pi \times 0.02$ Å^{-1}. The truncation criteria for electronic and ionic steps were chosen to be 10^{-5} eV and 10^{-2} eV/Å, respectively. Optimization of the graphene lattice parameters was performed for each atomic configuration (see Table 2) before commencing optimization of atomic positions. Some previous theoretical studies have indicated that the choice of an exchange-correlation functional can play an important role in defining adsorption energies of reaction intermediates over graphene-based single-atom catalysts (SACs).[31,32] Therefore, we have also run some tests using the PBE + *U* approach. The obtained results presented below suggest that the main conclusions of our study remain valid.

Acknowledgements

We acknowledge funding support from the National Science Foundation (NSF) through the NSF CAREER award (Grant No. CBET-1941204). R.B. is grateful to E-IMR and CRDAM centers at the Institute for Materials Research, Tohoku University, for continuous support. This research used resources of the National Energy Research Scientific Computing Center, a DOE Office of Science User Facility supported by the Office of Science of the U.S. Department of Energy under Contract No. DE-AC02-05CH11231, as well as the Holland Computing Center at the University of Nebraska-Lincoln.

Conflict of Interest

The authors declare no conflict of interest.

Data Availability Statement

The data that support the findings of this study are available from the corresponding author upon reasonable request.

Keywords: Single-atom catalysts · Dual-atom catalysts · Electrocatalysis · Hydrogen peroxide formation · Water oxidation reaction

[1] J. M. Campos-Martin, G. Blanco-Brieva, J. L. G. Fierro, *Angew. Chem. Int. Ed.* **2006**, *45*, 6962.
[2] S. C. Perry, D. Pangotra, L. Vieira, L.-I. Csepei, V. Sieber, L. Wang, C. Ponce de León, F. C. Walsh, *Nat. Chem. Rev.* **2019**, *3*, 442.
[3] S. Siahrostami, S. J. Villegas, A. H. Bagherzadeh Mostaghimi, S. Back, A. B. Farimani, H. Wang, K. A. Persson, J. Montoya, *ACS Catal.* **2020**, *10*, 7495.
[4] X. Shi, S. Back, T. M. Gill, S. Siahrostami, X. Zheng, *Chem* **2021**, *7*, 38.
[5] C. M. Sánchez-Sánchez, A. J. Bard, *Anal. Chem.* **2009**, *81*, 8094, pMID: 19725556.
[6] S. Siahrostami, A. Verdaguer-Casadevall, M. Karamad, D. Deiana, P. Malacrida, B. Wickman, M. Escudero-Escribano, E. A. Paoli, R. Frydendal, T. W. Hansen, I. Chorkendorff, I. E. L. Stephens, J. Rossmeisl, *Nat. Mater.* **2013**, *12*, 1137.
[7] Y. Shiraishi, S. Kanazawa, Y. Sugano, D. Tsukamoto, H. Sakamoto, S. Ichikawa, T. Hirai, *ACS Catal.* **2014**, *4*, 774.
[8] A. Verdaguer-Casadevall, D. Deiana, M. Karamad, S. Siahrostami, P. Malacrida, T. W. Hansen, J. Rossmeisl, I. Chorkendorff, I. E. L. Stephens, *Nano Lett.* **2014**, *14*, 1603, pMID: 24506229.
[9] S. Rojas-Carbonell, K. Artyushkova, A. Serov, C. Santoro, I. Matanovic, P. Atanassov, *ACS Catal.* **2018**, *8*, 3041.
[10] Y. Sun, L. Silvioli, N. R. Sahraie, W. Ju, J. Li, A. Zitolo, S. Li, A. Bagger, L. Arnarson, X. Wang, T. Moeller, D. Bernsmeier, J. Rossmeisl, F. Jaouen, P. Strasser, *J. Am. Chem. Soc.* **2019**, *141*, 12372, pMID: 31306016.
[11] N. Wang, X. Zhao, R. Zhang, S. Yu, Z. H. Levell, C. Wang, S. Ma, P. Zou, L. Han, J. Qin, L. Ma, Y. Liu, H. L. Xin, *ACS Catal.* **2022**, *12*, 4156.
[12] J. Liu, Y. Zou, B. Jin, K. Zhang, J. H. Park, *ACS Energy Lett.* **2019**, *4*, 3018.
[13] S. Y. Park, H. Abroshan, X. Shi, H. S. Jung, S. Siahrostami, X. Zheng, *ACS Energy Lett.* **2019**, *4*, 352.
[14] S. R. Kelly, X. Shi, S. Back, L. Vallez, S. Y. Park, S. Siahrostami, X. Zheng, J. K. Nørskov, *ACS Catal.* **2019**, *9*, 4593.
[15] X. Shi, S. Siahrostami, G.-L. Li, Y. Zhang, P. Chakthranont, F. Studt, T. F. Jaramillo, X. Zheng, J. K. Nørskov, *Nat. Commun.* **2017**, *8*, 701.
[16] X. Zhao, Y. Liu, *J. Am. Chem. Soc.* **2021**, *143*, 9423.
[17] S. Back, J. Na, Z. W. Ulissi, *ACS Catal.* **2021**, *11*, 2483.
[18] S. Siahrostami, G.-L. Li, V. Viswanathan, J. K. Nørskov, *J. Phys. Chem. Lett.* **2017**, *8*, 1157, pMID: 28231706.
[19] A. S. Varela, W. Ju, A. Bagger, P. Franco, J. Rossmeisl, P. Strasser, *ACS Catal.* **2019**, *9*, 7270.
[20] Y. He, S. Liu, C. Priest, Q. Shi, G. Wu, *Chem. Soc. Rev.* **2020**, *49*, 3484.
[21] W. Wang, Q. Jia, S. Mukerjee, S. Chen, *ACS Catal.* **2019**, *9*, 10126.
[22] E. F. Holby, G. Wang, P. Zelenay, *ACS Catal.* **2020**, *10*, 14527.
[23] T. Patniboon, H. A. Hansen, *ACS Catal.* **2021**, *11*, 13102.
[24] B. Singh, M. B. Gawande, A. D. Kute, R. S. Varma, P. Fornasiero, P. McNeice, R. V. Jagadeesh, M. Beller, R. Zbořil, *Chem. Rev.* **2021**, *121*, 13620, pMID: 34644065.
[25] H. Hu, J. Wang, P. Tao, C. Song, W. Shang, T. Deng, J. Wu, *J. Mater. Chem. A* **2022**, *10*, 5835.
[26] M. Xiao, Y. Chen, J. Zhu, H. Zhang, X. Zhao, L. Gao, X. Wang, J. Zhao, J. Ge, Z. Jiang, S. Chen, C. Liu, W. Xing, *J. Am. Chem. Soc.* **2019**, *141*, 17763, pMID: 31603677.
[27] H. Goto, Y. Hanada, T. Ohno, M. Matsumura, *J. Catal.* **2004**, *225*, 223.
[28] J. Zhang, Y. Nosaka, *J. Phys. Chem. C* **2013**, *117*, 1383.
[29] S. R. Kelly, X. Shi, S. Back, L. Vallez, S. Y. Park, S. Siahrostami, X. Zheng, J. K. Nørskov, *ACS Catal.* **2019**, *9*, 4593.
[30] S. Siahrostami, M. E. Björketun, P. Strasser, J. Greeley, J. Rossmeisl, *Phys. Chem. Chem. Phys.* **2013**, *15*, 9326.
[31] I. Barlocco, L. A. Cipriano, G. Di Liberto, G. Pacchioni, *Adv. Theory Simul.* **2022**, page 2200513.
[32] G. Di Liberto, L. A. Cipriano, G. Pacchioni, *ACS Catal.* **2022**, *12*, 5846.
[33] S. L. Dudarev, G. A. Botton, S. Y. Savrasov, C. Humphreys, A. P. Sutton, *Phys. Rev. B* **1998**, *57*, 1505.
[34] J. Gao, H. b Yang, X. Huang, S.-F. Hung, W. Cai, C. Jia, S. Miao, H. M. Chen, X. Yang, Y. Huang, T. Zhang, B. Liu, *Chem* **2020**, *6*, 658.
[35] J. S. Jirkovský, I. Panas, E. Ahlberg, M. Halasa, S. Romani, D. J. Schiffrin, *J. Am. Chem. Soc.* **2011**, *133*, 19432, pMID: 22023652.
[36] Y.-C. Lin, P.-Y. Teng, C.-H. Yeh, M. Koshino, P.-W. Chiu, K. Suenaga, *Nano Lett.* **2015**, *15*, 7408, pMID: 26488153.
[37] Y. Huang, Y. Chen, M. Xu, T. Asset, P. Tieu, A. Gili, D. Kulkarni, V. De Andrade, F. De Carlo, H. S. Barnard, A. Doran, D. Y. Parkinson, X. Pan, P. Atanassov, I. V. Zenyuk, *Mater. Today* **2021**, *47*, 53.
[38] B. B. Sarma, F. Maurer, D. E. Doronkin, J.-D. Grunwaldt, *Chem. Rev.* **2023**, *123*, 379,pMID: 36418229.
[39] G. Kresse, J. Furthmüller, *Phys. Rev. B* **1996**, *54*, 11169.
[40] G. Kresse, J. Furthmüller, *Comput. Mater. Sci.* **1996**, *6*, 15.
[41] G. Kresse, D. Joubert, *Phys. Rev. B* **1999**, *59*, 1758.
[42] J. P. Perdew, K. Burke, M. Ernzerhof, *Phys. Rev. Lett.* **1996**, *77*, 3865.
[43] Y. Zhang, W. Yang, *Phys. Rev. Lett.* **1998**, *80*, 890.
[44] S. Grimme, J. Antony, S. Ehrlich, H. Krieg, *J. Chem. Phys.* **2010**, *132*, 154104.
[45] V. Wang, N. Xu, J.-C. Liu, G. Tang, W.-T. Geng, *Comput. Phys. Commun.* **2021**, *267*, 108033.

Manuscript received: January 19, 2023
Revised manuscript received: March 16, 2023
Accepted manuscript online: March 16, 2023
Version of record online: ■■, ■■

RESEARCH ARTICLE

Single Atom Catalysts: Metal-nitrogen-graphene based single- and dual-atom catalysts are screened for high activity/selectivity in 2-electron water oxidation reaction. Several chemistries such as containing NiN_x–C moieties are predicted to match best-performing metal oxides.

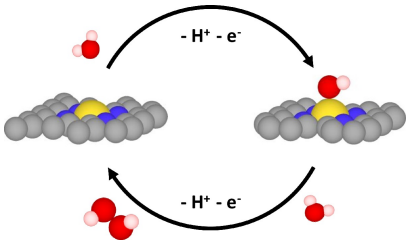

*P. Chaudhary, Dr. I. Evazzade, Prof. Dr. R. Belosludov, Prof. Dr. V. Alexandrov**